CMS Physics Analysis Summary

Contact: cms-pag-conveners-susy@cern.ch 2016/08/04

Search for new physics in final states with two opposite-sign, same-flavor leptons, jets, and missing transverse momentum in pp collisions at $\sqrt{s}$ = 13 TeV

The CMS Collaboration

Abstract

A search is presented for physics beyond the standard model in final states with two opposite-sign, same-flavor leptons, jets, and missing transverse momentum. The data sample corresponds to an integrated luminosity of 12.9 fb^{-1} of proton-proton collisions at $\sqrt{s} = 13$ TeV collected with the CMS detector at the LHC in 2016. The analysis uses the invariant mass of the lepton pair, searching for a kinematic edge or a resonant-like excess compatible with the Z boson mass. The search for a kinematic edge targets strong production while the resonance search targets both strongly and electroweakly produced new physics. Both search modes use several event categories in order to increase the sensitivity to new physics. These categories are based on several observables related to the lepton pair and the hadronic system in order to optimize signal efficiency and background rejection. A fit is employed to search for a possible kinematic edge position in the strong, non-resonant search. In addition, signal regions are included for which excesses were reported by the ATLAS and CMS collaborations using $\sqrt{s} = 8$ TeV and $\sqrt{s} = 13$ TeV data. The observations in all signal regions are consistent with the expectations from the standard model, and the results are interpreted in the context of simplified models of supersymmetry.

1 Introduction

Supersymmetry (SUSY) [1–8] is one of the most appealing extensions of the standard model (SM) and assumes a new fundamental symmetry that assigns a new fermion (boson) to every SM boson (fermion). SUSY resolves the hierarchy problem of the SM by stabilizing the Higgs boson mass via additional quantum loop corrections from the top super-partner (top squark), which compensate the correction due to the top quark. If R-parity [9] is conserved the lightest state predicted by the theory is stable and potentially massive, providing a candidate for dark matter. Many SUSY models also lead to the unification of the electroweak and strong forces at high energies [10–12].

This document presents a search for signatures of SUSY in events with two opposite-sign, same-flavor leptons (electrons or muons), jets, and missing transverse momentum. A data set of pp collisions collected with the CMS detector at the CERN LHC at $\sqrt{s} = 13\,\text{TeV}$ in 2016 was used, corresponding to an integrated luminosity of 12.9 fb^{-1}. The dilepton topology is expected to occur in SUSY models where a neutralino decays to either an on-shell Z boson or a virtual Z/γ boson which in turn decays to leptons and the lightest SUSY particle (LSP), or into a lepton and its supersymmetric partner (slepton), the latter decaying into another lepton and the LSP. Decays involving an on-shell Z boson are expected to produce an excess of events in which the di-lepton invariant mass is compatible with the Z boson mass, while decays involving off-shell Z bosons or sleptons are expected to produce a characteristic edge shape in the invariant mass distribution of the dilepton system [13].

The search for a contribution at the Z boson mass is performed in both scenarios of strong and electroweak SUSY production and features corresponding signal models and event selections. In case of the strong production, the neutralino is part of a decay chain starting from a gluino or squark, while in the electroweak case it is directly produced. The search for a kinematic edge is only performed under the assumption of strongly produced SUSY.

The CMS Collaboration published versions of this analysis using a $\sqrt{s} = 8\,\text{TeV}$ data set and a $\sqrt{s} = 13\,\text{TeV}$ data set from 2015. At 8 TeV a 2.6 σ local significance excess compatible with an edge shape located at a dilepton invariant mass of $78.7 \pm 1.4\,\text{GeV}$ [14] was observed. This excess could not be confirmed using 13 TeV data [15]. The ATLAS collaboration reported the absence of any excess in a similar signal region, but observed a 3.0 σ excess in dilepton events compatible with the Z boson mass in 8 TeV data [16] and 2.2 σ excess using 13 TeV data in 2015 [17]. A similar signal region in the CMS search at 13 TeV did not show any deviation from the expectation. Both deviations are analyzed here with minimal changes with respect to the previous 8 and 13 TeV searches.

2 The CMS detector

The central feature of the CMS apparatus is a superconducting solenoid, 13 m in length and 6 m in diameter, that provides an axial magnetic field of 3.8 T. The bore of the solenoid is outfitted with various particle detection systems. Charged-particle trajectories are measured by silicon pixel and strip trackers, covering $0 < \phi < 2\pi$ in azimuth and $|\eta| < 2.5$, where the pseudorapidity η is defined as $\eta = -\log[\tan(\theta/2)]$, with θ being the polar angle of the trajectory of the particle with respect to the beam direction. A crystal electromagnetic calorimeter (ECAL), and a brass and scintillator hadron calorimeter surround the tracking volume. The calorimetry provides high resolution energy and direction measurements of electrons and hadronic jets. A preshower detector consisting of two planes of silicon sensors interleaved with lead is located in front of the ECAL at $|\eta| > 1.479$. Muons are measured in gas-ionization detectors embedded

in the steel flux-return yoke outside the solenoid. The detector is nearly hermetic, allowing for energy balance measurements in the plane transverse to the beam direction. A two-tier trigger system selects the most interesting pp collision events for use in physics analysis. A more detailed description of the CMS detector, its coordinate system, and the main kinematic variables used in the analysis can be found elsewhere [18].

3 Datasets, triggers, and object selection

Events are collected with a set of dilepton triggers that require a transverse momentum of $p_T > 17$ or 23 GeV for the leading lepton depending on the time of data taking, except for the dimuon trigger where the requirement is always $p_T > 17$ GeV. These triggers impose loose isolation criteria on the leptons. For the subleading electron (muon) $p_T > 12$ (8) GeV is required and both leptons have to satisfy $|\eta| < 2.5$ (2.4) for electrons (muons). In order to retain high signal efficiency, in particular for Lorentz-boosted dilepton systems, dilepton triggers without isolation requirement have been used, which require for both leptons $p_T > 33$ (30) GeV in the dielectron (electron muon) case and either $p_T > 27$ (8) GeV or $p_T > 30$ (11) GeV for the leading (subleading) muon in dimuon events. The trigger efficiencies are measured in data using events selected by a suite of hadronic triggers.

Events are selected by requiring two opposite-charge, same-flavor leptons ($e^{\pm}e^{\mp}$ or $\mu^{\pm}\mu^{\mp}$) with $p_T > 25$ (20) GeV for the leading (subleading) lepton and pseudorapidity $|\eta| < 2.4$ for both leptons. The distance between the leptons must satisfy $\sqrt{\Delta\phi^2 + \Delta\eta^2} = \Delta R > 0.1$ to avoid reconstruction efficiency differences between electrons and muons in events with very collinear leptons. To ensure symmetry in acceptance between electrons and muons, all events with at least one of these two leptons in the barrel-endcap transition region of the ECAL, $1.4 < |\eta| < 1.6$, are rejected. A control sample of different flavor leptons ($e\mu$ or μe) is defined using the same lepton selection criteria. All the parameters above have been chosen in order to maximize the lepton selection efficiency while keeping the electron and muon efficiencies similar.

Electrons, reconstructed by associating tracks with ECAL clusters, are identified using a multivariate approach based on information on the cluster shape in the ECAL, track quality, and the matching between the track and the ECAL cluster [19]. Additionally, electrons from photon conversions are rejected. Muons are reconstructed from tracks found in the muon system associated with tracks in the tracker. They are identified based on the quality of the track fit and the number of associated hits in the tracking detectors. For both lepton flavors, the impact parameter with respect to the reconstructed vertex with the largest p_T^2 sum of associated tracks (primary vertex) is required to be within 0.5 mm in the transverse plane and below 1 mm along the beam direction. The lepton isolation, defined as the scalar p_T sum of all particle candidates, excluding the lepton itself, in a cone around the lepton, divided by the lepton p_T, is required to be smaller than 0.1 (0.2) for electrons (muons). A cone-size, varying with lepton p_T, is chosen to be $\Delta R = 0.2$ for $p_T < 50$ GeV, $\Delta R = 10\,\text{GeV}\,/\,p_T$ for $50 < p_T < 200$ GeV, and $\Delta R = 0.05$ for $p_T > 200$ GeV. This shrinking cone-size as a function of p_T recovers leptons from highly boosted decays.

In the electroweak search, additional electrons (muons) with an isolation of 0.4, $p_T > 10$ GeV and $|\eta| < 2.5$ (2.4) are vetoed.

A particle flow (PF) technique [20, 21] is used to reconstruct particle candidates in the event. Jets are clustered from these candidates, excluding charged hadrons not associated to the primary vertex, using the anti-k_t clustering algorithm [22] implemented in the FASTJET package [23, 24] with a distance parameter of 0.4. Each jet is required to have $p_T > 35$ GeV where the p_T is

corrected for non-uniform detector response and multiple collision (pileup) effects [25, 26], and $|\eta| < 2.4$. A jet is removed from the event if it lies within $\Delta R < 0.4$ of any of the selected leptons. The scalar sum of all jet transverse momenta is referred to as H_T. The magnitude of the negative vector p_T sum of all the PF candidates is referred to as E_T^{miss}. Corrections to the jet energy are propagated to the E_T^{miss} using the procedure developed for 7 TeV data [25]. Identification of jets originating from b-quarks is performed with the combined secondary vertex algorithm, using a working point in which the typical efficiency for b quarks is around 65% and the mis-tagging rate for light-flavor jets is around 1.5% [27].

While the main SM backgrounds are estimated using data control samples, simulated events are used to estimate uncertainties and minor SM background components. Next-to-leading order (NLO) and next-to-NLO cross sections [28–33] are used to normalize the simulated background samples, while NLO plus next-to-leading-logarithm (NLL) calculations [34] are used for the signal samples. Simulated samples of Drell-Yan (DY) production associated with jets (DY + jets), γ + jets, V + V, and $t\bar{t}V$ (V = W, Z) events are generated with the `MadGraph5_aMC@NLO` event generator [35], while `POWHEG` [36] is used for $t\bar{t}$ and single top quark production. The matrix element calculations performed with these generators are interfaced with PYTHIA 8 [37] for the simulation of parton showering and hadronization. The NNPDF3.0 parton distribution functions (PDF) [38] are used for all samples. The detector response is simulated with a GEANT4 model [39] of the CMS detector. The simulation of new physics signals is performed using the `MadGraph5_aMC@NLO` program at LO precision with up to 2 additional partons in the matrix element calculations. Events are then interfaced with PYTHIA 8 for fragmentation and hadronization, and simulated using the CMS fast simulation package [40]. Multiple pp interactions are superimposed on the hard collision and the simulated samples are reweighted such that the number of collisions per bunch crossing accurately reflects what is seen in data. Normalization scale factors are applied to the simulated samples to account for differences between simulation and data in the trigger and reconstruction efficiencies.

4 Signal models

This search targets different production and decay modes of neutralinos resulting in final states with two opposite-sign, same-flavor leptons; jets; and E_T^{miss} originating from the LSPs. In order to study these processes, three simplified models have been considered: two for the search for strongly produced SUSY, and one for the search for electroweakly produced SUSY.

One of the strong signal models as well as the electroweakly produced model produce a resonant lepton signature through an on-shell Z boson, while the other strong signal model results in an edge-like distribution in the invariant mass of the leptons targeted by the "edge" search.

The first of these simplified models represents gauge mediated supersymmetry breaking SUSY models [41] and is referred to as the GMSB scenario. The model assumes the production of a pair of gluinos ($\tilde{g}$) that decay into a pair of quarks (u, d, s, c, or b) and the lightest neutralino $\tilde{\chi}_1^0$. This neutralino decays into an on-shell Z boson and a massless gravitino ($\tilde{G}$) as seen in Fig. 1 (left). At least one of the Z bosons decays promptly into a pair of leptons producing the signature targeted by the strong on-Z search.

The signal model for the edge search, referred to as slepton-edge, assumes the production of a pair of bottom squarks, which decay to the next-to-lightest neutralino $\tilde{\chi}_2^0$ and a b quark. Two decay modes of the $\tilde{\chi}_2^0$ are considered each with 50% probability. In the first one, the $\tilde{\chi}_2^0$ decays to a Z boson and the lightest neutralino $\tilde{\chi}_1^0$, which is stable. The Z boson can be on- or off-shell,

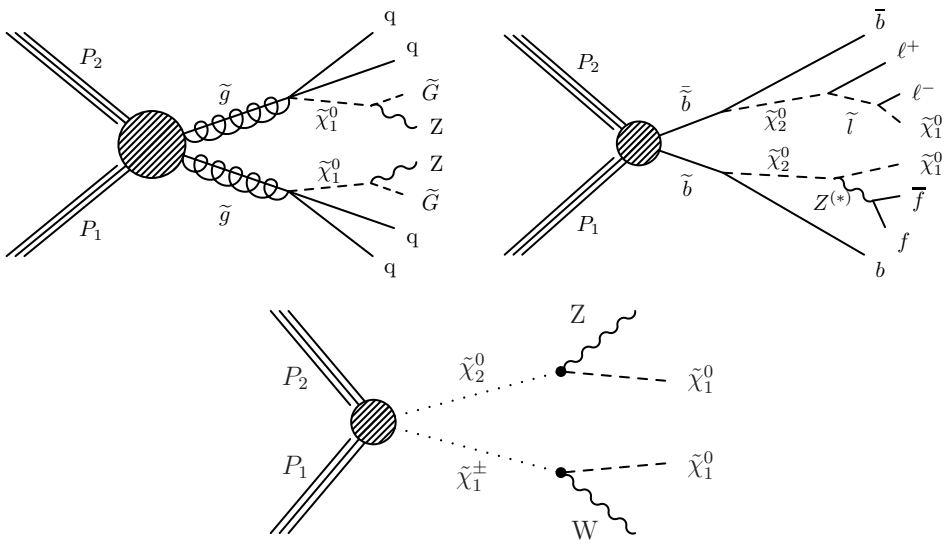

Figure 1: Diagrams for gluino and $\tilde{b}$ pair production and decays realized in the simplified models (top row). The GMSB model targeted by the strong on-Z search is shown on the left. On the right, the slepton-edge model features characteristic edges in the $m_{\ell\ell}$ spectrum given by the mass difference of the $\tilde{\chi}_2^0$ and $\tilde{\chi}_1^0$. The electroweak production model EWK-WZ (bottom) shows the production of a $\tilde{\chi}_2^0$ together with a $\tilde{\chi}_1^\pm$, resulting in a final state with a Z, and a W boson and two $\tilde{\chi}_1^0$ s.

depending on the mass difference between the neutralinos, and decays according to its SM branching fractions. The second one features sequential two-body decays with an intermediate slepton $\tilde{\ell}$: $\tilde{\chi}_2^0 \to \tilde{\ell}\ell \to \ell\ell\tilde{\chi}_1^0$. The masses of the sleptons ($\tilde{e}$, $\tilde{\mu}$) are assumed degenerate and equal to the average of the $\tilde{\chi}_2^0$ and $\tilde{\chi}_1^0$. The masses of the $\tilde{b}$ and $\tilde{\chi}_2^0$ are free parameters, while $m_{\tilde{\chi}_1^0}$ is fixed at 100 GeV. This scheme allows the position of the signal edge to vary along the invariant mass distribution according to the mass difference between the $\tilde{\chi}_2^0$ and $\tilde{\chi}_1^0$. The mass of the $\tilde{\chi}_1^0$ has been chosen in such a way that the difference to the $\tilde{\chi}_2^0$ mass is above 50 GeV, setting the minimum possible edge position at 50 GeV. An example for one of the possible decays is shown in Fig. 1 (right).

The simplified model for the electroweak search, referred to as the EWK-WZ model, can be seen in the bottom of Fig. 1. It shows the production of a $\tilde{\chi}_2^0$ and the lightest chargino $\tilde{\chi}_1^\pm$, which decay into a $\tilde{\chi}_1^0$ and a Z, and a $\tilde{\chi}_1^0$ and a W boson, respectively. The masses of the $\tilde{\chi}_2^0$ and $\tilde{\chi}_1^\pm$ are assumed to be equal in this simplified model.

5 Signal regions

The signal regions are designed to provide sensitivity to a range of new physics models, including the simplified models defined above. In the case of the strong on-Z and the edge search, an additional signal region is included to investigate excesses seen by the ATLAS collaboration when analyzing the 8 TeV data set [16] and the 13 TeV data set collected in 2015 [17]. Finally, a signal region designed to investigate the excess seen by the CMS collaboration when analyzing the 8 TeV data set [14] is also included in this analysis. The selections described below are applied in addition to the dilepton selection described in Section 3.

5.1 On-Z signal regions

The on-Z search is divided into a total of three signal region (SR) categories with dilepton invariant mass ($m_{\ell\ell}$) in the range $81 < m_{\ell\ell} < 101\,\text{GeV}$. The first two, referred to as "SRA" (2–3 jets and $H_\text{T} > 400\,\text{GeV}$) and "SRB" ($\geq 4$ jets), focus on events with low and high jet multiplicity. These categories are further divided according to the number of b-tagged jets, H_T, and E_T^miss.

One additional signal region, namely "ATLAS SR", is defined corresponding to the region showing a 2.2 σ excess in the 13 TeV data set of the ATLAS Collaboration [16]. This corresponds to an increased lepton-p_T threshold of 50 (25) GeV for the leading (subleading) lepton, the quantity $(H_\text{T} + p_\text{T}{}^{\ell_1} + p_\text{T}{}^{\ell_2}) > 600\,\text{GeV}$, $E_\text{T}^\text{miss} > 225$ GeV, and a selection on the $\Delta\phi$ between each of the leading jets and the E_T^miss of > 0.4.

The exact selection details for all signal regions are given along with the final results in Table 5.

5.2 Electroweak search signal regions

The signal region in the electroweak search also requires a dilepton pair with $81 < m_{\ell\ell} < 101\,\text{GeV}$, $E_\text{T}^\text{miss} > 150\,\text{GeV}$, and at least two jets. Events with any additional loosely isolated leptons with $p_\text{T} > 10\,\text{GeV}$ or b-tagged jets with $p_\text{T} > 25\,\text{GeV}$ are vetoed. In order to further suppress $\text{t}\bar{\text{t}}$ backgrounds, a requirement on M_{T2} [42, 43], a kinematic variable introduced to measure the mass of pair-produced particles decaying to the same visible and invisible particle, is introduced. When building M_{T2} from both leptons and E_T^miss, the distribution exhibits a sharp decline around the mass of the W-boson and is therefore well suited to suppress remaining contributions of $\text{t}\bar{\text{t}}$. The final requirement on M_{T2} is chosen to be 80 GeV. Furthermore, an additional requirement on the $|\Delta(\phi)|$ between E_T^miss and the largest-p_T jet of > 1 is implemented to further suppress fake-E_T^miss from DY processes. The signal region is then divided into three bins in E_T^miss: 150 – 225 GeV, 225 – 300 GeV, and above 300 GeV.

5.3 Edge search signal regions

The baseline signal region in the edge search requires $m_{\ell\ell} > 20\,\text{GeV}$, at least two jets, and $E_\text{T}^\text{miss} > 150\,\text{GeV}$. The fit to search for a kinematic edge in the invariant dilepton mass spectrum is performed in this baseline region. To perform a counting experiment this region is further subdivided into two $m_{\ell\ell}$ regions, the low mass region with $m_{\ell\ell} < 81\,\text{GeV}$ and the high mass region which requires $m_{\ell\ell} > 101\,\text{GeV}$, thereby excluding any overlap with the on-Z signal regions. A likelihood discriminant, NLL, is used to distinguish between events that most likely originate from dileptonically decaying top quark pairs and those that are not.

The observables used for the likelihood discriminator are: E_T^miss, the p_T of the dilepton system, $|\Delta(\phi)|$ between the leptons, and an observable called $\Sigma m_{\ell\text{b}}$. To calculate $\Sigma m_{\ell\text{b}}$, all combinations of leptons and jets are selected and the minimum mass is found. This process is repeated for the remaining lepton and jets, and the sum of the masses of the two systems is then defined as $\Sigma m_{\ell\text{b}}$. If b-tagged jets are present, they are given priority in the calculation of both lepton-jet systems; i.e. if one or two (or more) b-jets are present, $\Sigma m_{\ell\text{b}}$ between the leptons and the b-jets is minimized first, and then the remaining (b-)jets are considered for the minimization of the sum $\Sigma m_{\ell\text{b}}$ of the second lepton. To calculate this likelihood, the probability density functions of the four observables are determined by fits in the opposite-flavor control sample in the same kinematic region as the same-flavor signal region. The respective fit functions for the variables are a sum of two exponentials for the E_T^miss, a second-order polynomial for the $|\Delta(\phi)|$, and a Crystal-Ball function for both the di-lepton p_T as well as the $\Sigma m_{\ell\text{b}}$ distribution.

A likelihood function is then constructed and its negative logarithm is taken as the discrimi-

nator value NLL. Two categories of events are then defined, namely events that are $\mathrm{t\bar{t}}$-like and those that are non-$\mathrm{t\bar{t}}$-like. The distinction between the two categories is made such that the two bins have an expected $\mathrm{t\bar{t}}$ efficiency of 5% and 95%.

This results in a total of four cut-and-count signal regions: two bins in the $m_{\ell\ell}$ times two bins in the NLL discriminator.

In addition, one signal region corresponding to the signal region where the excess was observed by CMS at 8 TeV [14] is defined called the "CMS legacy" signal region. This region requires both leptons to be reconstructed in the central part of the detector ($|\eta| < 1.4$), $20 < m_{\ell\ell} < 70\,\mathrm{GeV}$, and $E_{\mathrm{T}}^{\mathrm{miss}} > 100\,(150)\,\mathrm{GeV}$ if at least three (two) jets are present.

A summary of all signal regions is given along with the experimental results in Section 8.

6 Standard model background predictions

The backgrounds from SM processes are divided into two types. Those that produce opposite-flavor (OF) pairs ($\mathrm{e}^{\pm}\mu^{\mp}$) as often as same-flavor (SF) pairs ($\mu^{\pm}\mu^{\mp}$, $\mathrm{e}^{\pm}\mathrm{e}^{\mp}$) are referred to as flavor-symmetric (FS) backgrounds. Among them, the dominant contribution arises from top quark-antitop quark production; sub-leading contributions from $\mathrm{W^+W^-}$, $Z/\gamma^*(\rightarrow \tau\tau)$, tW single-top quark production, and leptons from hadron decays are also present. The other category of backgrounds includes flavor-correlated lepton production and only contributes with SF leptons. The dominant contributions arise from DY production in association with jets, where the $E_{\mathrm{T}}^{\mathrm{miss}}$ arises from mismeasurement of the jet energies. Smaller contributions come from WZ and ZZ production, as well as rare processes such as $\mathrm{t\bar{t}Z}$. These backgrounds are referred to as "Other SM" in this document.

6.1 Flavor-symmetric backgrounds

The method of estimating the FS backgrounds relies on the fact that for such processes, SF and OF are produced at the same rate at particle level. This allows for the translation from the OF sample to the SF sample by application of an appropriate translation factor. For a scenario where the OF contribution is of sufficient statistical power to make an accurate prediction in the SF channel, this translation factor only has to correct for different flavor-dependent efficiencies stemming from reconstruction and identification effects and from flavor-dependent trigger efficiencies which might be different for electrons and muons.

A background estimate in the SF channel can therefore be obtained by simply applying a multiplicative correction factor, $R_{\mathrm{SF/OF}}$, to the OF channel yield. This factor is determined in two independent ways purely on collision data and then combined by weighting the two measurements according to their corresponding uncertainties. The two ways are a direct measurement of this translation factor in a control region outside of the baseline signal region on the one hand, and a factorized approach of measuring the effects of reconstruction, identification, and trigger separately on the other hand.

The direct measurement is performed in the region with $N_{\mathrm{jets}} = 2$ and $100 < E_{\mathrm{T}}^{\mathrm{miss}} < 150\,\mathrm{GeV}$, excluding the mass range $70 < m_{\ell\ell} < 110\,\mathrm{GeV}$ to reduce contributions from DY backgrounds. Here, $R_{\mathrm{SF/OF}}$ is evaluated using the observed yield of SF and OF events, $R_{\mathrm{SF/OF}} = \mathrm{N_{SF}}/\mathrm{N_{OF}}$. The applicability of this value in the signal region is confirmed by comparing it with the $R_{\mathrm{SF/OF}}$ value obtained in the signal region for $\mathrm{t\bar{t}}$ simulated events. The difference between both values is found to be similar to its statistical uncertainty (1%). The latter value is assigned as the systematic uncertainty in the measurement.

For the factorized approach, the ratio of muon to electron reconstruction and identification efficiencies, $r_{\mu/e}$, is measured in a DY-enriched region with $N_{\text{jets}} \geq 2$ and $E_{\text{T}}^{\text{miss}} < 50\,\text{GeV}$ and requiring $60 < m_{\ell\ell} < 120\,\text{GeV}$, resulting in a large sample of $e^{\pm}e^{\mp}$ and $\mu^{\pm}\mu^{\mp}$ events with similar kinematics to the signal region in terms of jet multiplicity. Assuming the factorization of lepton efficiencies in an event, the efficiency ratio is measured as $r_{\mu/e} = \sqrt{N_{\mu^+\mu^-}/N_{e^+e^-}}$. A systematic uncertainty of 10% is assigned to $r_{\mu/e}$ based on studies of its dependency on the lepton kinematics, the amount of $E_{\text{T}}^{\text{miss}}$, and the jet multiplicity. The trigger efficiencies for the three different flavor combinations are used to define the factor $R_{\text{T}} = \sqrt{\epsilon^T_{\mu^{\pm}\mu^{\mp}}\epsilon^T_{e^{\pm}e^{\mp}}}/\epsilon^T_{e^{\pm}\mu^{\mp}}$, which takes into account the difference between SF and OF channels at the trigger level. The final correction is $R_{\text{SF/OF}} = \frac{1}{2}(r_{\mu/e} + r^{-1}_{\mu/e}) \cdot R_{\text{T}}$. Here, $r_{\mu/e}$ is summed with its inverse, leading to a large reduction of the associated uncertainty. R_{T} is calculated only on collision data.

The results of the direct measurement and the factorization method are shown in Table 1. Since the results are in agreement and are obtained on independent data samples, they are combined using the weighted average. The resulting correction is $R_{\text{SF/OF}} = 1.09 \pm 0.02$.

Table 1: Summary of $R_{SF/OF}$ values obtained in data and simulation using the direct and factorized methods, and the final combination by weighting the two results according to their uncertainties.

	Data	MC
$\frac{1}{2}(r_{\mu/e} + r_{\mu/e}{}^{-1})$	1.032±0.025	1.020±0.020
R_T	1.062±0.069	-
$R_{\text{SF/OF}}$		
From factorization method	1.096±0.076	1.083±0.073
From direct measurement	1.090±0.024	1.101±0.003
Weighted average	1.091±0.023	1.101±0.003

6.1.1 Adaptations to the FS background prediction for the electroweak search

This method works well in searches in signal regions which feature a relatively large number of events. This is to say, the statistical uncertainty on the predicted number of events is driven by the Poisson error on the number of events in the OF control region. For regions with a very small number of expected events, such as the signal region for the electroweak searches, this method is no longer feasible and requires some adaptation in order to obtain a stable estimation of the FS background contribution. Since the search regions for the electroweak SUSY production employ a veto on b-tagged jets as well as the requirement of the invariant mass of the two leptons to be within 10 GeV of the Z-boson mass, this gives two lever arms to increase the statistical power of the prediction method. By extending the control region from the b-veto region to a region with at least one b-tagged jet, and by extending the window in $m_{\ell\ell}$ by 20 GeV on each side of the signal region the number of events in the OF control region is increased substantially. In order to translate this into a prediction for the SF signal region, it is needed to measure two additional multiplicative factors to be multiplied with $R_{\text{SF/OF}}$, namely the fraction of events on-Z over the number of events in the extended $m_{\ell\ell}$-window called f_{mll}, and the ratio of number of events with a b-veto over the number of events with b-tagged jets, called $r_{0\text{b}1\text{b}}$. These factors are determined from the OF control sample in MC simulation and validated in their respective data control regions, where good agreement is observed. Values of 0.33 ± 0.02 for f_{mll}, and 0.28 ± 0.02 for $r_{0\text{b}1\text{b}}$ are obtained and summarized in Table 2. Sta-

tistical uncertainties on these ratios are small, and systematic uncertainties stemming from the difference in these ratios in the OF and SF region are small as well.

Table 2: Measured values of f_{mll} and r_{0b1b}. Values are obtained from MC simulation after validating them on collision data.

quantity	value
f_{mll}	0.32 ± 0.02
r_{0b1b}	0.28 ± 0.02

An additional systematic uncertainty is assigned to the adapted method for the FS background prediction in the electroweak searches by performing a MC closure test in the tails of the $E_{\text{T}}^{\text{miss}}$ spectrum of the $\text{t}\bar{\text{t}}$ process. This systematic uncertainty is determined to be 30%.

6.2 Drell–Yan-like backgrounds

6.2.1 $E_{\text{T}}^{\text{miss}}$ template method

The $E_{\text{T}}^{\text{miss}}$ from the DY background is estimated from $E_{\text{T}}^{\text{miss}}$ templates obtained from a data control region. The main premise of this estimate based on data is that $E_{\text{T}}^{\text{miss}}$ in $\text{Z}+\text{jets}$ events originates from the limited detector resolution when measuring the objects making up the hadronic system that recoils against the Z boson. We estimate the shape of the $E_{\text{T}}^{\text{miss}}$ distribution from a control sample of $\gamma+\text{jets}$ events where the jet system recoils against a photon instead of a Z boson. Signal regions requiring at least one b-tagged jet can lead to a small amount of additional $E_{\text{T}}^{\text{miss}}$ due to the neutrinos in semileptonic b quark decays. To account for this effect, the $E_{\text{T}}^{\text{miss}}$ templates are extracted from a control sample of $\gamma+\text{jets}$ events with at least one b-tagged jet.

The $\gamma+$ jets events in data are selected with a suite of single-photon triggers with p_{T} thresholds varying from 22 to 165 GeV. The triggers with thresholds below 165 GeV are prescaled such that only a fraction of accepted events are recorded, and the events are weighted by the trigger prescales to match the integrated luminosity collected with the signal dilepton triggers. In order to account for kinematic differences between the hadronic systems in the $\gamma+\text{jets}$ and the $\text{Z}+\text{jets}$ sample, the $\gamma+\text{jets}$ sample is reweighted such that the boson p_{T} distribution matches that of the $\text{Z}+\text{jets}$ sample. This reweighting is performed for each signal region, where the same requirements are applied to the $\text{Z}+\text{jets}$ and the $\gamma+\text{jets}$ samples.

For the signal regions for the electroweak search, where a requirement on M_{T2} is implemented, this method has to be adapted since M_{T2} requires two visible objects, whereas the single photon in the $\gamma+\text{jets}$ does not suffice this criteria. Therefore, a method was developed to emulate this cut in $\gamma+\text{jets}$ by decaying the photon to two leptons. This method is described in detail in section 6.2.2. The resulting $E_{\text{T}}^{\text{miss}}$ distribution is then normalized to the observed data yield in a region where $\text{Z}+\text{jets}$ is the dominant background. For the electroweak signal region, this is defined to be the region with $50 < E_{\text{T}}^{\text{miss}} < 100$ GeV, and for every other signal region the normalization is performed in events with $E_{\text{T}}^{\text{miss}} < 50$ GeV.

The control sample used to estimate this background does not need to have a high purity of photons, since the $E_{\text{T}}^{\text{miss}}$ is assumed to originate from jet mismeasurement. However, it is required that the photon-like object be well measured so as to not contribute to the $E_{\text{T}}^{\text{miss}}$ mismeasurement. The stability of the photon selection is tested by repeating this background measurement after tightening the photon ID requirements, and it is found that the results are consistent

with the measurement done using the looser selection. In order to ensure the photon-like object is sufficiently well-measured and that the $E_{\mathrm{T}}^{\mathrm{miss}}$ in the $\gamma+$jets sample comes primarily from the mismeasurement of the jet system, the following conditions are required: $\Delta\phi(E_{\mathrm{T}}^{\mathrm{miss}}, \gamma) > 0.4$, a veto on events where the photon can be connected to a pattern of hits in the pixel detector, and the photon to be matched to a jet within a cone of ΔR = 0.4. Finally, the electromagnetic fraction of this jet, i.e. the fraction of jet energy deposited in the electromagnetic calorimeter with respect to the total energy deposited in both, the electromagnetic and hadronic calorimeter is required to be > 0.7.

The dominant uncertainties in the $E_{\mathrm{T}}^{\mathrm{miss}}$ template prediction come from the limited size of the samples used. The uncertainty in the prediction takes into account the statistical uncertainty of the $\gamma+$jets sample in the signal $E_{\mathrm{T}}^{\mathrm{miss}}$ regions, which ranges from 10–75 %. The statistical uncertainty of the normalization for $E_{\mathrm{T}}^{\mathrm{miss}} < 50$ GeV is included and ranges from 1–11%, as shown in Table 3. A closure test of the method is performed in simulation, using $\gamma+$jets to predict the yield of Z + jets. An uncertainty is assigned from the results of this test as either the largest discrepancy between the $\gamma+$jets prediction and the Z + jets yield for each $E_{\mathrm{T}}^{\mathrm{miss}}$ region, or the MC statistical uncertainty, whichever is larger. The values are listed in Table 4 and vary between 1 and 35%, depending on the $E_{\mathrm{T}}^{\mathrm{miss}}$ region.

6.2.2 M_{T2} emulation for the $E_{\mathrm{T}}^{\mathrm{miss}}$-template method

Two visible objects are needed when calculating the M_{T2} variable, and only one photon is required in the $\gamma+$jets events used to predict the $E_{\mathrm{T}}^{\mathrm{miss}}$ from the Z + jets background in the electroweak signal region. Therefore in order to emulate the M_{T2} cut in the $\gamma+$jets sample, a method was developed where the photon is decayed to two leptons and M_{T2} is calculated using the two decayed leptons as the visible objects. This decay is done by assuming the mother particle has the mass of a Z boson and the momentum of the photon reconstructed from data. The angular distribution of the leptons is accounted for by assuming a scenario where the direction of the spin of the mother particle is sampled from a distribution that is flat in $(1 + \cos^2(\theta))$, where θ is the polar angle in the system of reference in which the mother particle is at rest. After the photon is decayed, the same p_{T} and η requirements that are applied to the Z + jets events are applied to the decay products from the photon. M_{T2} is constructed using these leptons, and the same cut is applied, namely $M_{T2} > 80$ GeV. Finally, the p_{T} distribution is reweighted in the same way as is done in the other signal regions described in the previous section.

6.2.3 Correcting electroweak contamination in tails of $E_{\mathrm{T}}^{\mathrm{miss}}$ templates

After selecting events with a high-p_{T} photon and large $E_{\mathrm{T}}^{\mathrm{miss}}$, events from electroweak processes with real $E_{\mathrm{T}}^{\mathrm{miss}}$, e.g. W$\gamma$ where the W decays to $\ell\nu$, can be present in the tail of the $E_{\mathrm{T}}^{\mathrm{miss}}$ distribution. A cut is applied to the $\gamma+$jets data sample vetoing events that contain an isolated track identified by particle flow as a lepton or charged hadron with $p_{\mathrm{T}} > 5$ GeV to reduce the contamination from these electroweak processes. We then subtract the residual electroweak contamination after applying this selection, where the predicted value of this contamination is taken from MC after applying all the same selections including the aforementioned lepton veto. The difference between the prediction with and without the electroweak contamination subtracted is then applied as an additional systematic uncertainty on the final template prediction.

Table 3: Statistical uncertainties in the normalization of the $E_{\mathrm{T}}^{\mathrm{miss}}$ template prediction in the $E_{\mathrm{T}}^{\mathrm{miss}} < 50\,\mathrm{GeV}$ range (50 - 100 GeV for the electroweak signal region), for each signal region. These are taken as a systematic uncertainty in the background prediction. The definitions of SRA, SRB, and ATLAS SR are found in Section 5.1 and Table 5.

Signal region	SRA		SRB		ATLAS	edge	electroweak
	b-veto	≥ 1 b-tag	b-veto	≥ 1 b-tag			
Uncertainty	2 %	5 %	2 %	4 %	2%	1%	5%

Table 4: Systematic uncertainties in percentage for the $E_{\mathrm{T}}^{\mathrm{miss}}$ template method from the MC closure test, shown for all the on-Z signal regions. The definitions of SRA, SRB, and ATLAS SR are found in Section 5.1 and Table 5.

$\mathrm{E}_{\mathrm{T}}^{\mathrm{miss}}$(GeV)	0 – 50	50 – 100	100 – 150	150 – 225	225 – 300	≥ 300
SRA, b-veto	2 %	10 %	20 %	20 %	20 %	25 %
SRA, with b-tags	1 %	5 %	20 %	20 %	40 %	40 %
SRB, b-veto	1 %	6 %	10 %	10 %	35 %	35 %
SRB, with b-tags	1 %	10 %	20 %	25 %	30 %	30 %
EWK Signal Region	25 %	2 %	10 %	10 %	10 %	15 %
ATLAS Signal Region	2 %	10 %	25 %	35 %	40 %	
edge Signal Region	1 %	5 %	5 %	7 %		

6.2.4 JZB method

In the ATLAS signal region, the jet-Z balance (JZB) [44] is used as a second method to estimate the Drell–Yan backgrounds, in order to have an orthogonal cross-check of the results obtained with the method described above using γ + jets sample.

A detailed description of the JZB method can be found in previous publications, such as Ref. [44]. In brief, JZB is a measure of the imbalance between the p_{T} of the Z/γ^* boson and the p_{T} of the recoiling hadronic system in DY + jets events and is defined as the scalar difference of the p_{T} of the two systems. Standard model DY + jets events equally populate negative and positive values of JZB, because non-zero JZB in these events arises from jet energy resolution effects, whereas in SUSY and $\mathrm{t\bar{t}}$ events, which contain genuine $E_{\mathrm{T}}^{\mathrm{miss}}$, JZB can be very asymmetric towards positive values because of the correlated production of the lepton pair and the undetected particles. Events with negative values of JZB mainly arise from DY + jets processes, with a small contribution from $\mathrm{t\bar{t}}$ production. Therefore, in order to estimate the DY + jets contribution in the signal region located at positive JZB values, the negative JZB events can be used. Contribution from $\mathrm{t\bar{t}}$ in the negative JZB region is subtracted from the corresponding negative-JZB OF sample in data.

Uncertainties arising from imperfect knowledge of the $R_{\mathrm{SF/OF}}$ factor (Table 1) when subtracting the $\mathrm{t\bar{t}}$ contribution are propagated to the final DY + jets estimate. This method also accounts for processes with DY$\rightarrow \ell^{\pm}\ell^{\mp} + X$, where X denotes other particles that might be present in the final state. The systematic uncertainty in the assumption that DY + jets events equally populate positive and negative values of JZB is evaluated in simulation by comparing the $E_{\mathrm{T}}^{\mathrm{miss}}$ distributions of events with JZB < 0 and JZB > 0.

A systematic uncertainty of 30 % is assigned to account for possible differences, dominated by the limited statistical precision of the MC sample.

6.2.5 Other standard model processes with a Z boson

Both the $E_{\mathrm{T}}^{\mathrm{miss}}$ template and JZB method only predict instrumental $E_{\mathrm{T}}^{\mathrm{miss}}$ from jet mismeasurement and thus do not include the genuine $E_{\mathrm{T}}^{\mathrm{miss}}$ from neutrinos expected in processes like W($\ell\nu$)Z($\ell\ell$), Z($\ell\ell$)Z($\nu\nu$), or rarer processes such as $\mathrm{t\bar{t}Z}$. These processes contribute a small fraction of the overall background and are determined with MC simulation. The MC prediction is compared to data in 3- and 4-lepton control regions. Good agreement is observed in the 3-lepton control region, and therefore a systematic uncertainty of 30 % is assigned to cover for the statistical precision of this test and remaining kinematic differences between the 3-lepton control region and the 2-lepton signal region. In the 4-lepton control region, the ZZ event count is scaled to the observed data, thereby extracting a scale factor of 1.35. This scale factor is the applied to the MC prediction in the signal region. A systematic uncertainty of 50 % is applied to this process to cover for the limited statistics and potential kinematic differences.

6.2.6 Drell–Yan background in the edge search

A procedure was designed to propagate the estimations obtained using the $E_{\mathrm{T}}^{\mathrm{miss}}$ templates for the on-Z regions to the off-Z – edge – signal regions. This contribution is very small, around the percent level of the total background in the edge signal regions. For this reason, a ratio $r_{\mathrm{out/in}}$ is measured in the DY-dominated control region where $r_{\mu/\mathrm{e}}$ is also obtained. The numerator of this ratio is the number of SF events outside of the Z boson mass window, while the denominator is the SF yield within this window. Opposite-flavor yields in both the numerator and denominator are subtracted from the respective same-flavor yields in order to correct for FS contributions in the region where $r_{\mathrm{out/in}}$ is measured. The final ratio is 6 % in the 8 TeV edge legacy region, 11 % in the low mass region and 6 % in the high mass region. The final contribution to the edge-like signal regions is then the on-Z prediction multiplied by this ratio for each of the signal regions. An uncertainty of 25 % is assigned to $r_{\mathrm{out/in}}$ to cover its dependencies on $E_{\mathrm{T}}^{\mathrm{miss}}$ and the jet multiplicity.

7 Kinematic fit

The search for an edge based on the fit method is performed using a simultaneous extended unbinned maximum likelihood fit to the dilepton mass distributions of $\mathrm{e^+e^-}$, $\mu^+\mu^-$, and $\mathrm{e^\pm}\mu^\mp$ events. The likelihood model contains three components: a) a FS background component, b) a DY background component, and c) a signal component.

The FS background is described using a Crystal-Ball [45] function: $\mathcal{P}_{CB}(m_{\ell\ell})$:

$$\mathcal{P}_{CB}(m_{\ell\ell}) = \begin{cases} \exp\left(-\frac{(m_{ll}-\mu_{CB})^2}{2\sigma_{CB}^2}\right) & \text{if } \frac{m_{ll}-\mu_{CB}}{\sigma_{CB}} < \alpha, \\ A(B+\frac{m_{ll}-\mu_{CB}}{\sigma_{CB}})^{-n} & \text{if } \frac{m_{ll}-\mu_{CB}}{\sigma_{CB}} > \alpha, \end{cases} \tag{1}$$

where

$$A = \left(\frac{n}{|\alpha|}\right)^n \exp\left(-\frac{|\alpha|^2}{2}\right) \quad \text{and} \quad B = \frac{n}{|\alpha|} - |\alpha|. \tag{2}$$

The DY background is modeled with the sum of an exponential function, which describes the low-mass rise, and a Breit–Wigner function with a mean and width set to the nominal Z boson values [46], which accounts for the on-Z lineshape. To account for the experimental resolution, the Breit–Wigner function is convolved with a double-sided Crystal-Ball [45] function

$\mathcal{P}_{DSCB}(m_{\ell\ell})$:

$$\mathcal{P}_{DSCB}(m_{\ell\ell}) = \begin{cases} A_1(B_1 - \frac{m_{ll}-\mu_{CB}}{\sigma_{CB}})^{-n_1} & \text{if } \frac{m_{ll}-\mu_{CB}}{\sigma_{CB}} < -\alpha_1, \\ \exp\left(-\frac{(m_{ll}-\mu_{CB})^2}{2\sigma_{CB}^2}\right) & \text{if } -\alpha_1 < \frac{m_{ll}-\mu_{CB}}{\sigma_{CB}} < \alpha_2, \\ A_2(B_2 + \frac{m_{ll}-\mu_{CB}}{\sigma_{CB}})^{-n_2} & \text{if } \frac{m_{ll}-\mu_{CB}}{\sigma_{CB}} > \alpha_2, \end{cases} \quad (3)$$

The full model for the on-Z DY lineshape is thus:

$$\mathcal{P}_{DY,\,\text{on-Z}}(m_{\ell\ell}) = \int \mathcal{P}_{DSCB}(m_{\ell\ell})\mathcal{P}_{BW}(m_{\ell\ell} - m')dm'. \quad (4)$$

The signal component is described by a triangular shape, convolved with a Gaussian distribution to account for the experimental resolution:

$$\mathcal{P}_S(m_{\ell\ell}) \propto \frac{1}{\sqrt{2\pi}\sigma_{\ell\ell}} \int_0^{m_{\ell\ell}^{edge}} y \cdot \exp\left(-\frac{(m_{\ell\ell}-y)^2}{2\sigma_{\ell\ell}^2}\right) dy. \quad (5)$$

As a preliminary step, a fit is performed separately for electrons and muons in the DY-enriched control region (the same control region as described for $r_{\text{out/in}}$ in Section 6.2.6) to determine the shape of backgrounds containing a Z boson. The parameters of the DY shape are then fixed and only the normalizations of these backgrounds are free parameters in the fit. The nominal fit is applied simultaneously to the dilepton invariant mass distributions in the e^+e^-, $\mu^+\mu^-$, and $e^\pm\mu^\mp$ samples in the baseline signal region. Therefore the model for the FS background is the same for the SF and OF events.

The $R_{\text{SF/OF}}$ factor is treated as a nuisance parameter, parametrized by Gaussian distributions with a mean value and standard deviation given by the value of $R_{\text{SF/OF}}$ and its uncertainties (Table 1).

The signal model has two free parameters: the fitted signal yield and the position of the edge.

8 Results

The observed number of events in the different signal regions is compared with the background estimates obtained with the methods explained above for the strong on-Z and the edge searches and the electroweak search. For the edge search, the kinematic fit is applied additionally to search for a kinematic edge in the $m_{\ell\ell}$ spectrum.

8.1 Results of the search for strong production

8.1.1 Results of the on-Z search for strong production

The results for the 16 exclusive signal regions of the strong on-Z search and the additional ATLAS signal region are presented in Table 5. A graphical representation of these results can be seen in Fig. 2, where the background prediction has been divided into its three components: FS, DY, and other processes with a Z boson, in order to illustrate their relative contributions in the different signal regions. No excess above the expectation from the background prediction is observed.

Table 5: Results for the strong on-Z search, binned as a function of H_T, the jet multiplicity, the b jet multiplicity, and the missing transverse momentum. In the ATLAS SR an additional requirement is imposed on the angle between the E_T^{miss} and the two leading jets $\Delta\phi_{E_T^{miss},j_1,j_2} > 0.4$ and the p_T thresholds of the leading (subleading) leptons are increased to 50 (25) GeV.

N_{jets} / H_T	$N_{b\text{-jets}}$	E_T^{miss} (GeV)	Predicted	Observed
SRA	0	100-150	$169.6\ ^{+16.1}_{-15.7}$	**177**
		150-225	$43.6\ ^{+7.1}_{-6.3}$	**45**
		225-300	$24.3\ ^{+12.7}_{-12.4}$	**11**
2–3 jets		> 300	$15.0\ ^{+4.8}_{-3.8}$	**23**
	≥ 1	100-150	$77.2\ ^{+9.2}_{-8.1}$	**87**
		150-225	$40.0\ ^{+7.4}_{-6.2}$	**34**
and $H_T > 400$ GeV		225-300	$12.0\ ^{+4.6}_{-3.4}$	**22**
		> 300	$11.5\ ^{+4.5}_{-3.3}$	**11**
SRB	0	100-150	$126.3\ ^{+12.5}_{-11.8}$	**122**
		150-225	$39.5\ ^{+7.0}_{-5.9}$	**45**
		225-300	$11.7\ ^{+4.4}_{-3.1}$	**11**
		> 300	$5.7\ ^{+3.3}_{-2.1}$	**7**
	≥ 1	100-150	$240.8\ ^{+18.9}_{-16.1}$	**238**
		150-225	$81.2\ ^{+10.7}_{-9.6}$	**99**
		225-300	$24.1\ ^{+6.1}_{-5.0}$	**24**
≥ 4 jets		> 300	$7.2\ ^{+3.9}_{-2.6}$	**7**
ATLAS - SR:				
$H_T + p_T^{\ell_1} + p_T^{\ell_2} > 600$ GeV	$E_T^{miss} > 225$ GeV	$\Delta\phi_{E_T^{miss},j_1,j_2} > 0.4$	$44.1\ ^{+8.4}_{-7.5}$	**51**

8.1.2 Results in the ATLAS signal region using JZB

Results for the ATLAS region using the alternative DY-estimation method with the JZB variables are presented in Fig. 3 where the JZB spectrum is shown for the predicted backgrounds and the observed data. The E_T^{miss} requirement of the ATLAS region is not applied here, as the JZB variable has the E_T^{miss} observable as an input.

In tabulated form, these JZB results are presented in Table 6. Good overall agreement is observed and therefore the ATLAS excess seen in 2015 cannot be confirmed by this result.

8.1.3 Results of the edge search

The edge-like search features two distinct $m_{\ell\ell}$ regions, each of which is divided into two bins using the leptonic likelihood, resulting in four signal regions. Table 7 summarizes the SM predictions and the observations in these signal regions. A graphical representation of these results is shown in Fig. 4, including the relative contributions of the different backgrounds.

The agreement between the prediction and the observed number of events is good for all regions but one, where an excess is observed above the SM expectations. This excess is of the

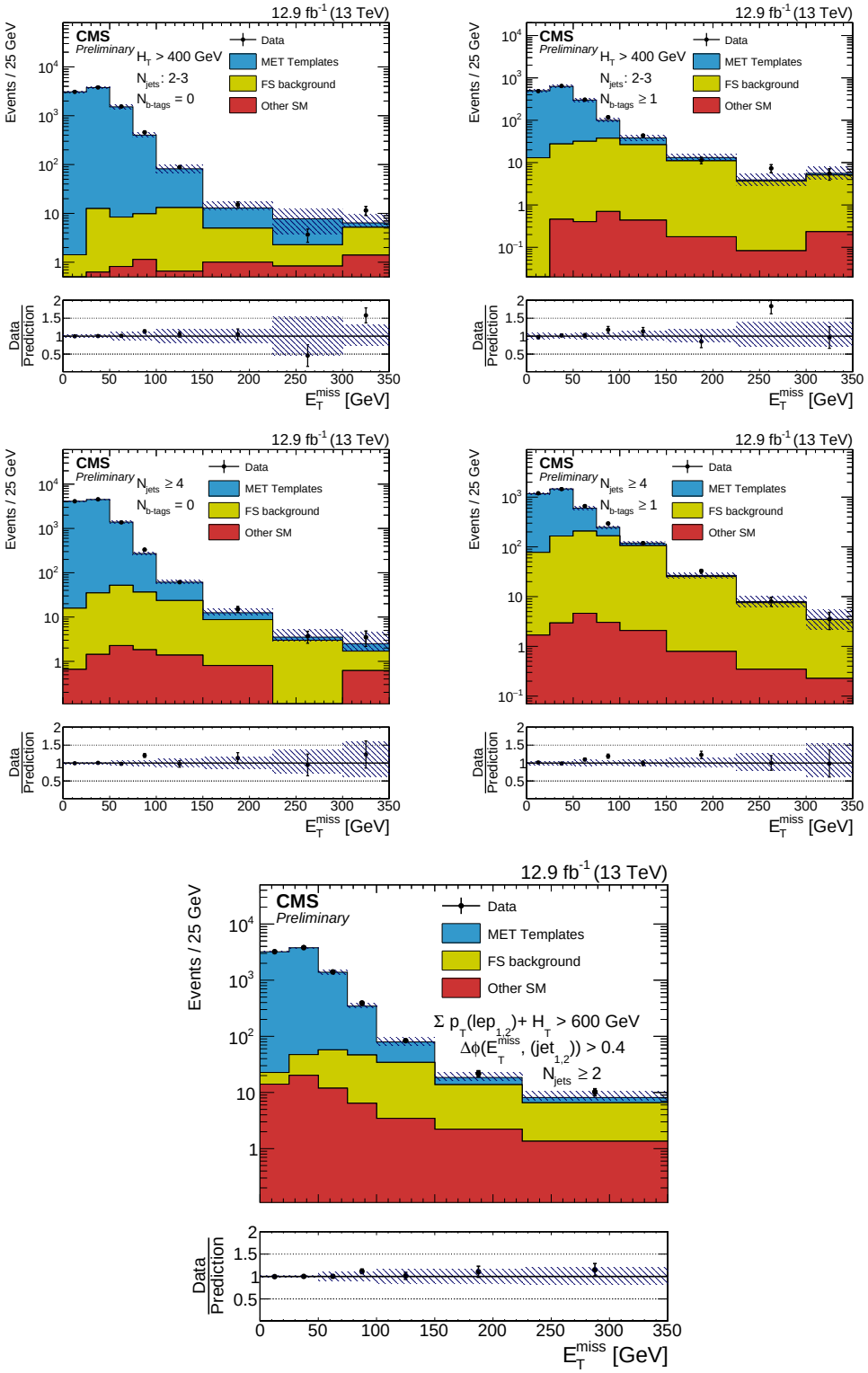

Figure 2: The $E_{\mathrm{T}}^{\mathrm{miss}}$ distribution is shown for data vs. the data-driven predictions in the on-Z signal regions and the ATLAS-like signal region. The plots on the left show the values when requiring $\mathrm{N_{b-jets}} = 0$, and the plots on the right show the values when requiring $\mathrm{N_{b-jets}} \geq 1$. The bottom plot shows the ATLAS-like signal region. See Table 5 for yields.

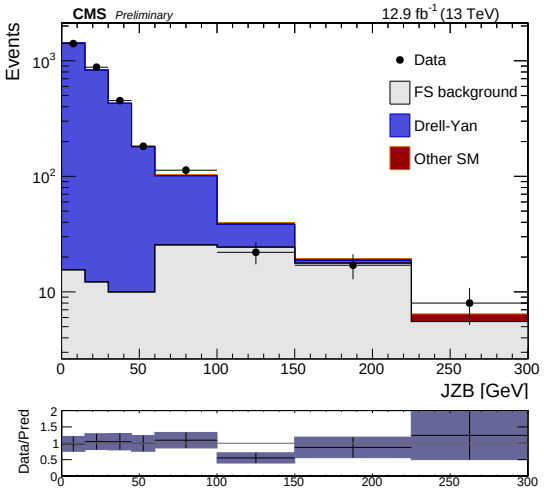

Figure 3: JZB spectrum for 12.9 fb^{-1} of collision data. Flavor symmetric backgrounds are shown in the gray histogram, the DY prediction using the negative JZB in blue and the observed data in black markers. The uncertainties on the background prediction are included in the ratio.

Table 6: Results in the ATLAS signal region using the JZB DY-prediction method.

FS background	$4.4\ ^{+3.5}_{-2.1}$
Drell-Yan	$0.0\ ^{+1.8}_{-0}$
Other SM	$1.7\ ^{+0.8}_{-0.8}$
Total background	$6.1^{+4.0}_{-2.2}$
Observed	8.0

order of 3.1 standard deviations, calculated as a local significance.

Figure 5 shows the $m_{\ell\ell}$ distribution for the "CMS legacy" signal region with central leptons CMS reported a moderate excess at $\sqrt{s} = 8$ TeV [14]. In this region 2170 signal events are observed while 2053$\pm$68 events were expected. This deviation corresponds to a local significance of 1.2 σ. Scaling the excess from 8 TeV by the luminosity and the ratio of cross sections between 13 TeV and 8 TeV and assuming that the excess was due to sbottom pair production would result in 342 (484, 654) events for sbottom masses of 300 (500, 700) GeV. Figure 5 shows the results for this signal region with the signal shape from 8 TeV data overlaid on top of the background prediction for these three sbottom mass scenarios. The signal shapes have been normalized to the expected event yields stated above.

The dilepton mass distributions and the results of the kinematic fit are shown in Fig. 6. Table 8 presents a summary of the fit results. A signal yield of 147.6 ± 78.9 events is obtained when evaluating the signal hypothesis in the baseline signal region, with an edge located at $132.0^{+3.9}_{-2.5}$ GeV. The test statistics $-2\ln Q$, where Q denotes the ratio of the fitted likelihood value for the signal-plus-background hypothesis to the background-only hypothesis, evaluated on data is compared to the respective quantity on a large sample of background only toy MC to estimate the p-value. The resulting p-value for a fixed edge position is 0.046 (local p-value) and 0.277 in case the edge position is allowed to float (global p-value). These p-values are interpreted as the one-sided tail probability of a Gaussian distribution and corresponds

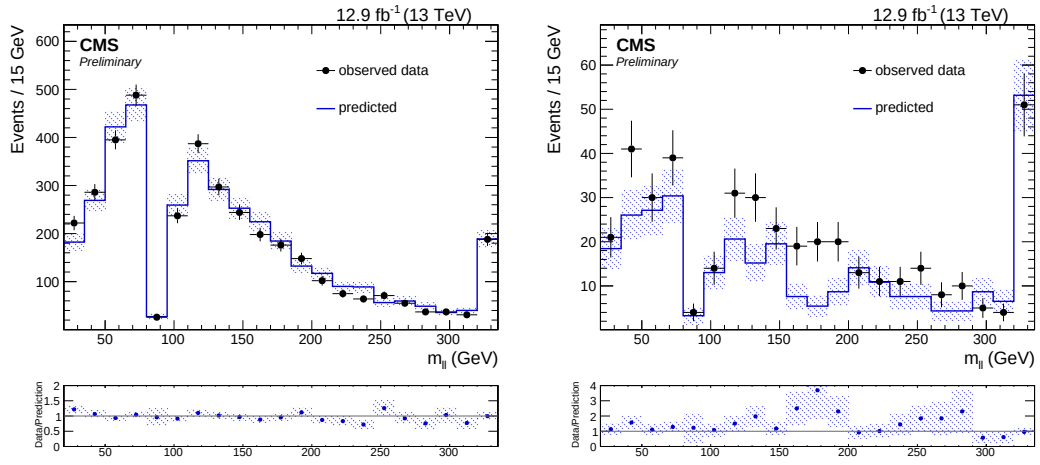

Figure 4: Overview of the results in the strong search shown in the $m_{\ell\ell}$ spectrum of the two leptons. The left plot shows the region with $\mathrm{t\bar{t}}$-like events while the right shows events which are classified as non-$\mathrm{t\bar{t}}$-like. The region left of the empty bin corresponds to the low mass region, the region right of it to high-mass.

Table 7: Predicted and observed results for the edge search in the four $m_{\ell\ell}$ versus NLL regions for 12.9 fb^{-1} of data.

		ttbar-like	non-ttbar-like
mll $<$ 81 GeV	pred. FS	1374.4 ± 48.1	105.8 ± 10.9
	pred. DY	13.5 ± 4.6	7.3 ± 2.5
	pred. total	1387.9 ± 48.3	113.1 ± 11.2
	obs	1417	135
mll $>$ 101 GeV	pred. FS	2435.8 ± 72.2	208.3 ± 15.7
	pred. DY	7.6 ± 2.6	4.1 ± 1.4
	pred. total	2443.4 ± 72.3	212.4 ± 15.7
	obs	2347	285

to an excess in the observed number of events compared to the SM background estimate of 2.0(1.1) σ local (global) standard deviations.

As a cross-check, we tested an alternative shape for the FS background that was used at 8 TeV. The results were found to be consistent with the nominal results.

8.2 Results of the electroweak search

Results of the electroweak regions are shown in Table 9 where the observations are compared to the background predictions in all three bins of $E_{\mathrm{T}}^{\mathrm{miss}}$. The resulting $E_{\mathrm{T}}^{\mathrm{miss}}$ spectrum is shown in Fig. 7. For the data analyzed, observations are found to be compatible with the expected yields from SM backgrounds.

Table 8: Results of the unbinned maximum likelihood fit for event yields in the signal region. The quoted uncertainties are calculated using the MINOS [47] program and account for both statistical and systematic sources.

Drell–Yan	177 ± 29
OF yield	4247 ± 59
$R_{\mathrm{SF/OF}}$	1.08 ± 0.02
Signal events	147.6 ± 78.9
$m_{\ell\ell}{}^{\mathrm{edge}}$	$132.0^{+3.9}_{-2.5}$ GeV
Local significance	$2.00\,\sigma$
Global significance	$1.09\,\sigma$

Table 9: Observations and predicted background yields for the electroweak signal regions for 12.9 fb^{-1}.

MET region	150 – 225 GeV	225 – 300 GeV	$\geq$ 300 GeV
Other rare	1.53 ± 0.79	0.80 ± 0.45	0.40 ± 0.23
WZ	7.01 ± 2.16	2.67 ± 0.85	2.61 ± 0.84
ZZ	4.20 ± 1.98	2.60 ± 1.36	2.03 ± 1.08
DY prediction	18.28 ± 2.91	4.69 ± 2.32	2.73 ± 1.56
$\mathrm{t\bar{t}}$	3.91 ± 1.36	0.50 ± 0.27	0.10 ± 0.11
Total bkg	34.9 ± 4.4	11.3 ± 2.9	7.9 ± 2.1
Observed	45	15	7

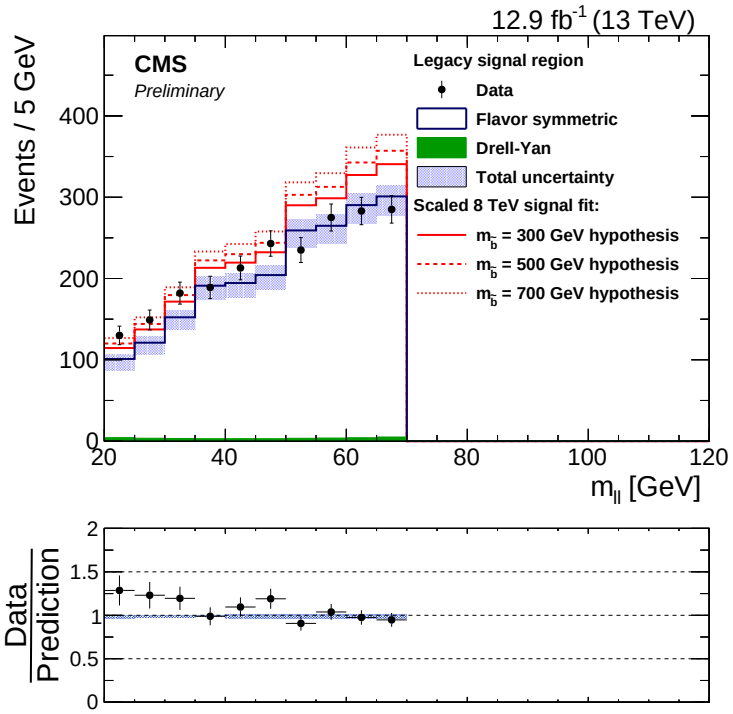

Figure 5: The $m_{\ell\ell}$ distribution is shown for the region where CMS reported an excess in Run 1. Data is displayed as black points, while the total background is shown as a solid blue line surrounded by a shaded blue band for the total uncertainty. The DY background contribution is shown in green. The signal shape measured by CMS with 8 TeV data has been overlaid on top of the background prediction. It has been normalized to the size of the excess observed at 8 TeV scaled by the ratio of integrated luminosity and cross section for three different sbottom mass hypothesis.

9 Interpretation

The results of the analysis are interpreted in terms of simplified models. In order to quantify the sensitivity of the on-Z and edge searches, two simulated samples with a scan of mass points of the GMSB and slepton-edge models have been produced. In the search for electroweak production, the EWK-WZ model is used. Upper limits on the cross section multiplied by the branching ratio have been calculated at a 95% confidence level (CL) using the CL_S criterion and an asymptotic formulation [48–51], taking into account the statistical and systematic uncertainties in the signal yields and the background predictions.

9.1 Systematic uncertainty in the signal yield

The systematic uncertainties in the signal yield have been evaluated by comparing the yields obtained after making a variation on the source of the systematic effect and the nominal yields. The uncertainty related to the measurement of the integrated luminosity is 6.2%. The uncertainty in the corrections used to account for lepton identification and isolation efficiency differences between data and simulation in an uncertainty of 7% in the signal acceptance. The uncertainty in the b tagging efficiency and mistag probability are 0-5%. A further systematic uncertainty of 4-5% is considered on the scale factors correcting for the differences between fast and GEANT4 simulations for leptons. Dilepton trigger efficiencies ranging between 90% and 97%, and depending on the lepton flavor, are measured in data and applied as an overall scale

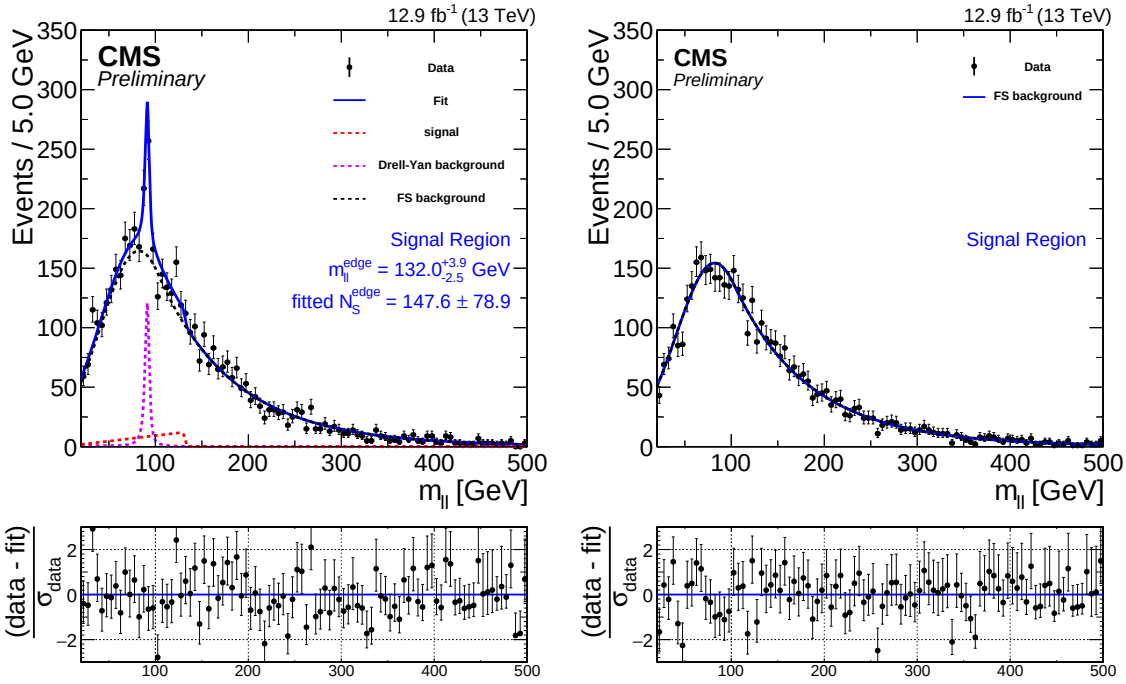

Figure 6: Fit results for the signal-plus-background hypothesis in comparison with the measured dilepton mass distributions, in the baseline signal region, projected on the same-flavor (left) and opposite-flavor (right) event samples. The combined fit shape is shown as a blue, solid line. The individual fit components are indicated by dashed lines. The flavor-symmetric (FS) background is displayed with a black dashed line. The Drell–Yan (DY) background is displayed with a purple dashed line. The extracted signal component is displayed with a red dashed line.

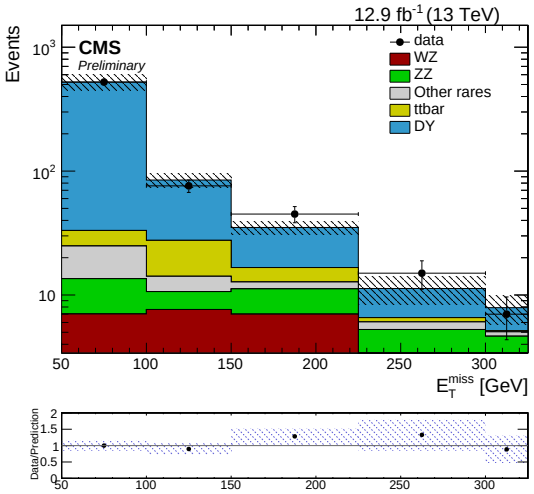

Figure 7: Distribution of $E_{\mathrm{T}}^{\mathrm{miss}}$ in the electroweak search region. The three final bins correspond to the final search regions used for the interpretation of the results.

factor to the signal simulation with a systematic uncertainty of 5%. The uncertainty in the jet energy scale varies between 1% and 5% depending on the signal kinematics. The uncertainty associated with the modeling of initial-state radiation (ISR) is 0-2% for most mass combinations and can reach up to 10% at the diagonal. The uncertainty in the correction to account for the pileup in the simulation is evaluated by shifting the inelastic cross section by $\pm$ 5% and amounts to 0-3% on signal acceptance. To account for uncertainties in $E_{\mathrm{T}}^{\mathrm{miss}}$ in fast simulation, the evaluation of the signal yield is repeated using generator $E_{\mathrm{T}}^{\mathrm{miss}}$. The average of both yields is used for the signal yields and the difference between this value and the yield using standard $E_{\mathrm{T}}^{\mathrm{miss}}$ is used as an uncertainty that ranges from 1-10%. Finally the statistical uncertainty on the number of simulated events is also considered and found to be in the range 1-9%, depending on the signal region and mass point. These uncertainties are summarized in Table 10.

Table 10: List of systematic uncertainties taken into account for the signal yields and typical values.

Source of uncertainty	Uncertainty (%)
Luminosity	6.2
Pileup	0-3
b tag modeling	0-5
Lepton reconstruction and isolation	7
Fast simulation scale factors	4-5
Fast simulation MET uncertainty	1-10
Trigger modeling	5
Jet energy scale	1-5
ISR modeling	0-10
Statistical uncertainty	1-9
Total uncertainty	12-16

9.2 Interpretation using simplified models

Since the GMSB model leads to a signature containing at least 6 jets in the final state, most of the sensitivity of the on-Z search is provided by the high jet multiplicity signal regions defined within the SRB category. We only consider the number of observed and predicted events in these regions to set limits on this model. The expected and observed limits are presented in Fig. 8. We exclude gluino masses up to 1.5 (1.3) TeV for large (small) neutralino masses. These results show an improvement with respect to the 2015 13 TeV result where we obtained an observed and expected limits for gluino masses from 1.03 to 1.28 TeV.

The edge search is interpreted using the slepton-edge model, combining the two invariant mass and likelihood regions. Figure 9 shows the exclusion contour in the plane of the masses of the bottom squark and the second neutralino. We exclude bottom squark masses up to 750 GeV. Due to the observed excess, the observed limit is about 50-150 GeV weaker than the expected limit. The decrease in sensitivity at a neutralino mass of $\sim$ 200–250 GeV corresponds to a kinematic edge located at $\sim$ 100–150 GeV. In this case, signal events frequently have an invariant mass close to the Z boson mass and do not fall into any of the $m_{\ell\ell}$ regions. For low (high) $\tilde{\chi}_2^0$ masses, the majority of signal events fall into the low- (high-) mass bin, which increases the sensitivity for these mass points.

9.2.1 Interpretations in the search for electroweak production

The search for electroweak production is interpreted using the EWK-WZ model and the observations and predictions in the three electroweak signal regions. Figure 10 shows the cross section upper limits and the exclusion lines at 95% CL for an assumed mass of 0 GeV. The analysis is sensitive for masses between 200 GeV and 330 GeV approximately, improving the results obtained with the 8 TeV data set. Due to the slight excess observed in the two lower $E_{\mathrm{T}}^{\mathrm{miss}}$ signal regions with respect to the background prediction, the observed limit does not exclude any of the masses in the range.

10 Summary

A search for physics beyond the standard model has been presented in the opposite-sign, same-flavor lepton; jets; and $E_{\mathrm{T}}^{\mathrm{miss}}$ final state using a data sample of pp collisions collected with the CMS detector in 2016 at a center-of-mass energy of 13 TeV, corresponding to an integrated luminosity of 12.9 fb^{-1}. Searches are performed for signals that either produce a kinematic edge in the dilepton invariant mass, or use dilepton systems whose invariant mass is compatible with the decay of a Z boson. Comparing the observation to estimates for SM backgrounds obtained from data control samples, no statistically significant evidence for a signal has been observed.

The search for strongly produced new physics containing an on-shell Z boson is interpreted in a model of gauge-mediated supersymmetry breaking, where the Z bosons are produced in decay chains initiated through gluino pair production, and where the branching ratios have been fixed to 100% to produce the desired topology. Gluino masses below 1300 TeV for high

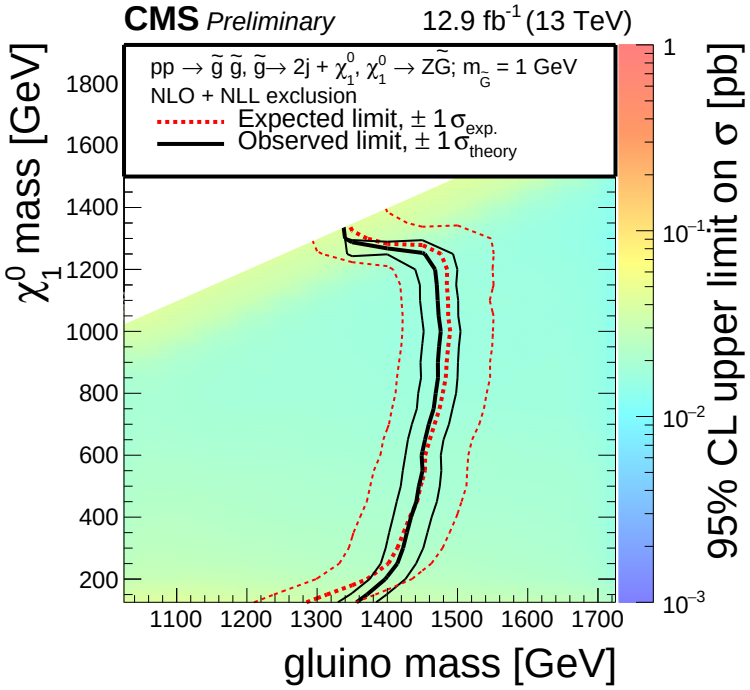

Figure 8: Cross section upper limits and exclusions contours at 95% CL with the results of the on-Z search interpreted in the GMSB model. The region to the left of the red dotted (black solid) line shows the masses which are excluded by the expected (observed) limit.

and low neutralino masses, and 1500 TeV for medium neutralino masses have been excluded, extending the previous exclusion limits derived from a similar analysis at 13 TeV by almost 200 GeV.

The search for an edge-like kinematic feature is interpreted in a simplified model based on bottom squark pair production, where dilepton mass edges are produced in decay chains containing the two lightest neutralinos and a slepton, where again the branching ratios have been fixed to produce the desired topology. Bottom squark masses below 800 and 625 GeV have been excluded, depending on the $\tilde{\chi}_2^0$ mass. These limits extend previous exclusion limits by about 150 GeV depending also on the $\tilde{\chi}_2^0$ mass.

The electroweak search has been interpreted in simplified models of chargino-neutralino production and neutralino-neutralino production where the neutralino decays to a Z boson and the LSP and the chargino decays to a W boson and the LSP. The search is sensitive to neutralino and chargino masses between 200 GeV and about 330 GeV, however due to a slight excess of the observation over the predicted estimates, the observed limit does not exclude any mass in the considered range.

The two event selections where excesses of 2.6 and 3.0 σ significance had been observed by the CMS and ATLAS collaborations in their respective 8 TeV results have been explored finding good agreement between the observation and the background prediction estimates.

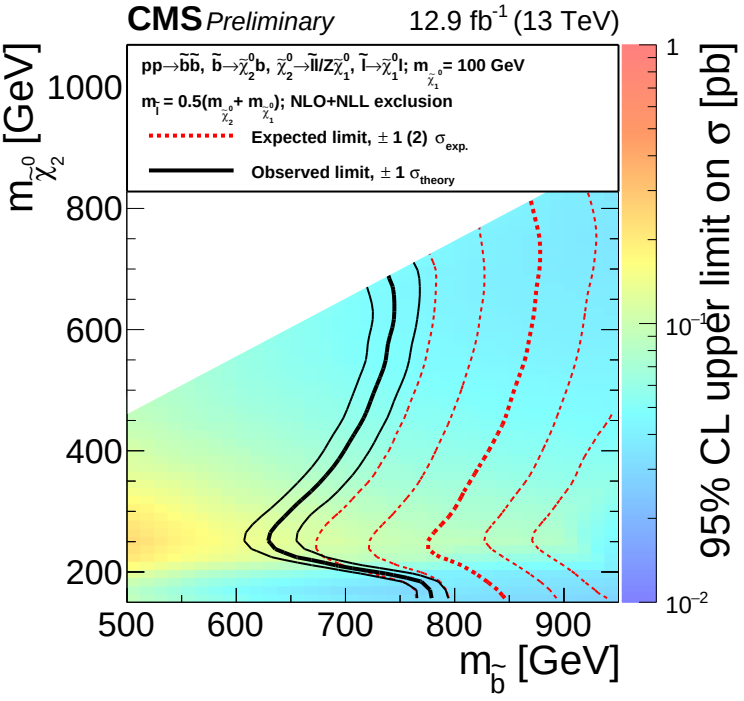

Figure 9: Cross section upper limits and exclusion contours at 95% CL with the results of the edge search interpreted in the slepton-edge model. The region to the left of the red dotted (black solid) line shows the masses which are excluded by the expected (observed) limit.

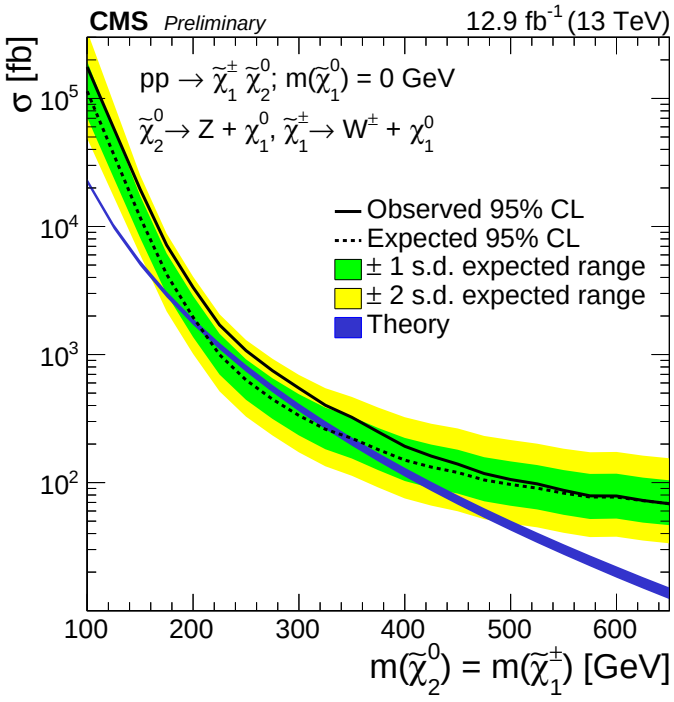

Figure 10: Cross section upper limits and exclusion lines at 95% CL for the search for electroweak production where the mass of the $\tilde{\chi}_1^0$ has been set to 0 GeV. Regions where the black dotted line reaches below the theoretical cross section (blue band) are expected to be excluded. The observed upper limit on the cross section is shown in a black solid line.

References

[1] P. Ramond, "Dual theory for free fermions", *Phys. Rev. D* **3** (1971) 2415, doi:10.1103/PhysRevD.3.2415.

[2] Y. A. Golfand and E. P. Likhtman, "Extension of the algebra of Poincaré group generators and violation of P invariance", *JETP Lett.* **13** (1971) 323.

[3] A. Neveu and J. H. Schwarz, "Factorizable dual model of pions", *Nucl. Phys. B* **31** (1971) 86, doi:10.1016/0550-3213(71)90448-2.

[4] D. V. Volkov and V. P. Akulov, "Possible universal neutrino interaction", *JETP Lett.* **16** (1972) 438.

[5] J. Wess and B. Zumino, "A Lagrangian model invariant under supergauge transformations", *Phys. Lett. B* **49** (1974) 52, doi:10.1016/0370-2693(74)90578-4.

[6] J. Wess and B. Zumino, "Supergauge transformations in four dimensions", *Nucl. Phys. B* **70** (1974) 39, doi:10.1016/0550-3213(74)90355-1.

[7] P. Fayet, "Supergauge invariant extension of the Higgs mechanism and a model for the electron and its neutrino", *Nucl. Phys. B* **90** (1975) 104, doi:10.1016/0550-3213(75)90636-7.

[8] H. P. Nilles, "Supersymmetry, supergravity and particle physics", *Phys. Rep.* **110** (1984) 1, doi:10.1016/0370-1573(84)90008-5.

[9] G. R. Farrar and P. Fayet, "Phenomenology of the Production, Decay, and Detection of New Hadronic States Associated with Supersymmetry", *Phys. Lett. B* **76** (1978) 575, doi:10.1016/0370-2693(78)90858-4.

[10] A. Buras, J. Ellis, M. Gaillard, and D. Nanopoulos, "Aspects of the grand unification of strong, weak and electromagnetic interactions", *Nuclear Physics B* **135** (1978), no. 1, 66, doi:http://dx.doi.org/10.1016/0550-3213(78)90214-6.

[11] H. Haber and G. Kane, "The search for supersymmetry: Probing physics beyond the standard model", *Physics Reports* **117** (1985), no. 2, 75, doi:http://dx.doi.org/10.1016/0370-1573(85)90051-1.

[12] H. Nilles, "Supersymmetry, supergravity and particle physics", *Physics Reports* **110** (1984), no. 1, 1, doi:http://dx.doi.org/10.1016/0370-1573(84)90008-5.

[13] I. Hinchliffe et al., "Precision SUSY measurements at CERN LHC", *Phys. Rev.* **D55** (1997) 5520, doi:10.1103/PhysRevD.55.5520, arXiv:hep-ph/9610544.

[14] CMS Collaboration, "Search for Physics Beyond the Standard Model in Events with Two Leptons, Jets, and Missing Transverse Momentum in pp Collisions at $\sqrt{s} = 8$ TeV", *JHEP* **04** (2015) 124, doi:10.1007/JHEP04(2015)124, arXiv:1502.06031.

[15] CMS Collaboration, "Search for new physics in final states with two opposite-sign, same-flavor leptons, jets and missing transverse momentum in pp collisions at $\sqrt{s} = 13$ TeV", arXiv:1607.00915.

[16] ATLAS Collaboration, "Search for supersymmetry in events containing a same-flavour opposite-sign dilepton pair, jets, and large missing transverse momentum in $\sqrt{s} = 8$ TeV pp collisions with the ATLAS detector", *Eur. Phys. J. C* **75** (2015) 318, doi:10.1140/epjc/s10052-015-3661-9, 10.1140/epjc/s10052-015-3518-2, arXiv:1503.03290. [Erratum: *Eur. Phys. J. C* **75** (2015) 463].

[17] ATLAS Collaboration, "A search for Supersymmetry in events containing a leptonically decaying Z boson, jets, and missing transverse momentum in $\sqrt{s} = 13$ TeV pp collisions with the ATLAS detector", Technical Report ATLAS-CONF-2015-082, CERN, 2015.

[18] CMS Collaboration, "The CMS experiment at the CERN LHC", *JINST* **3** (2008) S08004, doi:10.1088/1748-0221/3/08/S08004.

[19] CMS Collaboration, "Performance of electron reconstruction and selection with the CMS detector in proton-proton collisions at $\sqrt{s} = 8$ TeV", *JINST* **10** (2015) P06005, doi:10.1088/1748-0221/10/06/P06005, arXiv:1502.02701.

[20] CMS Collaboration, "Particle-Flow Event Reconstruction in CMS and Performance for Jets, Taus, and MET", Technical Report CMS-PAS-PFT-09-001, CERN, 2009. Geneva, Apr, 2009.

[21] CMS Collaboration, "Commissioning of the Particle-flow Event Reconstruction with the first LHC collisions recorded in the CMS detector", Technical Report CMS-PAS-PFT-10-001, 2010.

[22] M. Cacciari, G. P. Salam, and G. Soyez, "The anti-k_t jet clustering algorithm", *JHEP* **04** (2008) 063, doi:10.1088/1126-6708/2008/04/063, arXiv:0802.1189.

[23] M. Cacciari, G. P. Salam, and G. Soyez, "FastJet user manual", *Eur. Phys. J. C* **72** (2012) 1896, doi:10.1140/epjc/s10052-012-1896-2, arXiv:1111.6097.

[24] M. Cacciari and G. P. Salam, "Dispelling the N^3 myth for the k_t jet-finder", *Phys. Lett. B* **641** (2006) 57, doi:10.1016/j.physletb.2006.08.037, arXiv:hep-ph/0512210.

[25] CMS Collaboration, "Determination of Jet Energy Calibration and Transverse Momentum Resolution in CMS", *JINST* **6** (2011) P11002, doi:10.1088/1748-0221/6/11/P11002, arXiv:1107.4277.

[26] M. Cacciari and G. P. Salam, "Pileup subtraction using jet areas", *Phys. Lett. B* **659** (2008) 119, doi:10.1016/j.physletb.2007.09.077, arXiv:0707.1378.

[27] CMS Collaboration, "Identification of b quark jets at the CMS Experiment in the LHC Run 2", Technical Report CMS-PAS-BTV-15-001, 2016.

[28] J. Alwall et al., "The automated computation of tree-level and next-to-leading order differential cross sections, and their matching to parton shower simulations", *JHEP* **07** (2014) 079, doi:10.1007/JHEP07(2014)079, arXiv:1405.0301.

[29] S. Alioli, P. Nason, C. Oleari, and E. Re, "NLO single-top production matched with shower in POWHEG: s- and t-channel contributions", *JHEP* **09** (2009) 111, doi:10.1007/JHEP02(2010)011, 10.1088/1126-6708/2009/09/111, arXiv:0907.4076. [Erratum: *JHEP* **02** (2010) 011].

[30] E. Re, "Single-top Wt-channel production matched with parton showers using the POWHEG method", *Eur. Phys. J. C* **71** (2011) 1547, doi:10.1140/epjc/s10052-011-1547-z, arXiv:1009.2450.

[31] R. Gavin, Y. Li, F. Petriello, and S. Quackenbush, "FEWZ 2.0: A code for hadronic Z production at next-to-next-to-leading order", *Comput. Phys. Commun.* **182** (2011) 2388–2403, doi:10.1016/j.cpc.2011.06.008, arXiv:1011.3540.

[32] R. Gavin, Y. Li, F. Petriello, and S. Quackenbush, "W Physics at the LHC with FEWZ 2.1", *Comput. Phys. Commun.* **184** (2013) 208–214, doi:10.1016/j.cpc.2012.09.005, arXiv:1201.5896.

[33] M. Czakon and A. Mitov, "Top++: A Program for the Calculation of the Top-Pair Cross-Section at Hadron Colliders", *Comput. Phys. Commun.* **185** (2014) 2930, doi:10.1016/j.cpc.2014.06.021, arXiv:1112.5675.

[34] C. Borschensky et al., "Squark and gluino production cross sections in pp collisions at $\sqrt{s}$ = 13, 14, 33 and 100 TeV", *Eur. Phys. J. C* **74** (2014), no. 12, 3174, doi:10.1140/epjc/s10052-014-3174-y, arXiv:1407.5066.

[35] J. Alwall et al., "The automated computation of tree-level and next-to-leading order differential cross sections, and their matching to parton shower simulations", *JHEP* **07** (2014) 079, doi:10.1007/JHEP07(2014)079, arXiv:1405.0301.

[36] S. Frixione, P. Nason, and C. Oleari, "Matching NLO QCD computations with Parton Shower simulations: the POWHEG method", *JHEP* **11** (2007) 070, doi:10.1088/1126-6708/2007/11/070, arXiv:0709.2092.

[37] T. Sjostrand, S. Mrenna, and P. Z. Skands, "A Brief Introduction to PYTHIA 8.1", *Comput. Phys. Commun.* **178** (2008) 852–867, doi:10.1016/j.cpc.2008.01.036, arXiv:0710.3820.

[38] NNPDF Collaboration, "Parton distributions for the LHC Run II", *JHEP* **04** (2015) 040, doi:10.1007/JHEP04(2015)040, arXiv:1410.8849.

[39] GEANT4 Collaboration, "GEANT4 — a simulation toolkit", *Nucl. Instrum. Meth. A* **506** (2003) 250, doi:10.1016/S0168-9002(03)01368-8.

[40] S. Abdullin et al., "The fast simulation of the CMS detector at LHC", *J. Phys. Conf. Ser.* **331** (2011) 032049, doi:10.1088/1742-6596/331/3/032049.

[41] S. P. Martin, "A Supersymmetry primer", doi:10.1142/9789812839657_0001, 10.1142/9789814307505_0001, arXiv:hep-ph/9709356. [Adv. Ser. Direct. High Energy Phys.18,1(1998)].

[42] C. G. Lester and D. J. Summers, "Measuring masses of semiinvisibly decaying particles pair produced at hadron colliders", *Phys. Lett. B* **463** (1999) 99, doi:10.1016/S0370-2693(99)00945-4, arXiv:hep-ph/9906349.

[43] A. Barr, C. Lester, and P. Stephens, "A variable for measuring masses at hadron colliders when missing energy is expected; m T 2 : the truth behind the glamour", *J. Phys. G* **29** (2003) 2343, doi:10.1088/0954-3899/29/10/304, arXiv:hep-ph/0304226.

[44] CMS Collaboration, "Search for physics beyond the standard model in events with a Z boson, jets, and missing transverse energy in pp collisions at $\sqrt{s} = 7$ TeV", *Physics Letters B* **716** (2012) 260, doi:http://dx.doi.org/10.1016/j.physletb.2012.08.026.

[45] M. J. Oreglia, "A study of the reactions $\psi' \to \gamma\gamma\psi$". PhD thesis, Stanford University, 1980. SLAC Report SLAC-R-236, see Appendix D.

[46] Particle Data Group, J. Beringer et al., "Review of Particle Physics", *Phys. Rev. D* **86** (2012) 010001, doi:10.1103/PhysRevD.86.010001.

[47] F. James and M. Roos, "Minuit: A System for Function Minimization and Analysis of the Parameter Errors and Correlations", *Comput. Phys. Commun.* **10** (1975) 343, doi:10.1016/0010-4655(75)90039-9.

[48] T. Junk, "Confidence level computation for combining searches with small statistics", *Nucl. Instrum. Meth. A* **434** (1999) 435, doi:10.1016/S0168-9002(99)00498-2, arXiv:hep-ex/9902006.

[49] A. L. Read, "Presentation of search results: the CL_s technique", *J. Phys. G* **28** (2002) 2693, doi:10.1088/0954-3899/28/10/313.

[50] ATLAS and CMS Collaborations, "Procedure for the LHC Higgs boson search combination in summer 2011", Technical Report ATL-PHYS-PUB-2011-011, CMS-NOTE-2011-005, CERN, 2011.

[51] G. Cowan, K. Cranmer, E. Gross, and O. Vitells, "Asymptotic formulae for likelihood-based tests of new physics", *Eur. Phys. J. C* **71** (2011) 1554, doi:10.1140/epjc/s10052-011-1554-0, 10.1140/epjc/s10052-013-2501-z, arXiv:1007.1727. [Erratum: *Eur. Phys. J. C* **73** (2013) 2501].